Molecular layer deposition of alucone in high aspect ratio trenches: The effect of TMA outgassing on step-coverage

Cite as: J. Vac. Sci. Technol. A 41, 012401 (2023); https://doi.org/10.1116/6.0002249
Submitted: 26 September 2022 • Accepted: 03 November 2022 • Published Online: 06 December 2022

Hardik Jain, Mariadriana Creatore and 🗓 Paul Poodt

COLLECTIONS

Paper published as part of the special topic on Atomic Layer Deposition (ALD)









ARTICLES YOU MAY BE INTERESTED IN

Atomic layer deposition of conductive and semiconductive oxides
Applied Physics Reviews 9, 041313 (2022); https://doi.org/10.1063/5.0116732

Nucleation and growth mechanism for atomic layer deposition of Al_2O_3 on two-dimensional WS $_2$ monolayer

Journal of Vacuum Science & Technology A 41, 013201 (2023); https://doi.org/10.1116/6.0001913

Conformal chemical vapor deposition of boron-rich boron carbide thin films from triethylboron

Journal of Vacuum Science & Technology A 41, 013401 (2023); https://doi.org/10.1116/6.0002203







Molecular layer deposition of alucone in high aspect ratio trenches: The effect of TMA outgassing on step-coverage

Cite as: J. Vac. Sci. Technol. A 41, 012401 (2023); doi: 10.1116/6.0002249 Submitted: 26 September 2022 · Accepted: 3 November 2022 · Published Online: 6 December 2022







Hardik Jain, 1,2 Mariadriana Creatore, 2 and Paul Poodt 1,2,a) (D



- ¹TNO/Holst Centre, 5656 AE Eindhoven, Netherlands
- ²Department of Applied Physics, Eindhoven University of Technology, 5600 MB Eindhoven, Netherlands

Note: This paper is part of the 2023 Special Topic Collection on Atomic Layer Deposition (ALD).

a)Author to whom correspondence should be addressed: p.w.g.poodt@tue.nl

ABSTRACT

Infiltration of trimethylaluminum (TMA) in molecular layer deposition-enabled alucone thin films on planar substrates is a common observation reported in the literature. An insufficient TMA purge time in such cases is often found to lead to a CVD component in the overall film growth due to the reactions between the outgassing TMA and the co-reactant. In this work, the effect of the CVD component on the step coverage of alucone films when grown in high-aspect ratio trenches is studied. The thickness was initially found to increase with increasing distance from the trench aperture before starting to decrease up to the film's maximum penetration depth. With the support of modeling, the reason behind the observed thickness profile was investigated and attributed to the combination of an increasing outgassing rate of TMA and a decreasing ethylene glycol (EG) concentration along the trench depth. Furthermore, the maximum thickness and the position where it is obtained in the trench are found to depend on TMA and EG doses, TMA purge time, the trench height, and the trench depth. Finally, the possibility of adopting the additional CVD component in film growth for void-less gap fill of 3D trenches is discussed, as well as the suppression of the same CVD component, without compromising the growth rate, by using dimethylaluminum isopropoxide as a substitute for TMA is evaluated.

© 2022 Author(s). All article content, except where otherwise noted, is licensed under a Creative Commons Attribution (CC BY) license (http://creativecommons.org/licenses/by/4.0/). https://doi.org/10.1116/6.0002249

I. INTRODUCTION

Atomic layer deposition (ALD) is a thin film deposition method well known for its ability to deposit highly conformal films inside 3D and porous substrates with aspect ratios up to several thousands. Molecular layer deposition (MLD) shares the same principles of ALD but adopts organic precursors or coreactants to deposit organic and hybrid films. For similar reasons as in ALD, MLD has a great potential to deposit organic or hybrid films within high aspect ratio substrates for several applications, ranging from semiconductors to 3D batteries. Usually, the deposition rate, step coverage, and thickness profiles of ALD/MLD films in 3D structures are determined by the rates of diffusion and reaction of the precursor and coreactant inside the 3D structure. In some examples of MLD, however, there might be secondary effects

playing a significant role in determining the deposition rates and step coverage. One example is of alucone prepared using trimethy-laluminum (TMA) and ethylene glycol (EG) as a precursor and a co-reactant, respectively.

In alucone MLD on planar substrates using TMA and EG, TMA is known to not only participate in the surface MLD reactions but also infiltrate into the underlying film during the TMA exposure step. This is based on quartz crystal microbalance (QCM) studies where it was found that the mass-gain recorded by the QCM during the TMA's exposure step is much higher than what is needed to saturate surface reactions. The mass-gain was then observed to decay in the subsequent purge step stabilizing at a value much closer to what is expected for surface saturation indicating outgassing of the infiltrated TMA. It cannot be, however, excluded that a part of the infiltrated precursor could stay

permanently trapped within the film upon reaction with the bulk, and hence, even after very long purge steps, the steady-state mass gain/cycle value in some cases could be several times higher than needed for surface saturation.8 Nevertheless, the outgassing step of TMA was observed to take very long in most of the cases, sometimes between ten and several hundreds of seconds.⁶⁻⁹ It can be expected that such long purge steps will also be required when the alucone films are deposited within 3D structures and even more so as the TMA outgassing rate will be hampered by the 3D structure itself. In the case of insufficiently long purge times, TMA will continue to outgas during the EG dose leading to CVD-type reactions that will add to the overall growth per cycle (GPC). 6,7,9 In our earlier work on planar substrates, we found that the CVD component can be up to three times larger than the pure MLD component.9 These high values of GPC can be used to achieve high deposition rate MLD on planar substrates, as long as the CVD component is reproducible and does not lead to undesirable changes in the film properties. The effect of the CVD reactions on step coverage in 3D structures, however, is uncertain. Earlier work involving MLD of alucone on, e.g., particles, 6,10 polymeric fibers, 1 and nanowires¹² made use of very long purge times where CVD reactions were presumably absent.

In this work, we have investigated the effect of CVD reactions during MLD of alucone using TMA and EG within high aspect ratio structures. Lateral high aspect ratio (LHAR) structures are used as test substrates while the film thickness profiles were measured using reflectometry. A variety of complex thickness profiles has been observed, which could be explained with the help of a simple simulation model. Finally, possible mitigation of the outgassing of TMA to realize conformal growth and the use of outgassing in trench filling has been discussed.

II. EXPERIMENTAL DETAILS

Trimethylaluminum (TMA) from Akzo Nobel, ethylene glycol, 99.8% (EG) from Sigma Aldrich, and dimethylaluminum isopropoxide (DMAI) from Strem Chemicals were used as MLD reactants in this study. All three reactants were dosed using a dip-tube bubbler assembly. In depositing alucone films using TMA and EG, the TMA bubbler was kept at room temperature and the EG bubbler was heated to 80 °C, whereas for alucone depositions carried out using DMAI and EG, the DMAI bubbler was heated to 75 °C while the EG bubbler was heated to 100 °C. Partial pressures of the reactants were set by adjusting the carrier (Ar for TMA, N2 for EG) and dilution flows. All experiments in this work were performed using a rotary, atmospheric pressure spatial ALD/MLD setup described in detail before. ¹³ The temperature for all the depositions was set at 150 °C. A notation for the reactant exposure and purge times denoted by (t_1, t_2, t_3, t_4) has been used in this work where t_1 and t_3 are the exposure times of TMA and EG, respectively, whereas t_2 and t_4 are the purge times after TMA and EG pulses, respectively, in seconds.

To inspect the conformality of alucone films, PillarHall[®] LHAR trenches supplied by Chipmetrics Oy. were used as substrates. The trenches are enabled by a polysilicon membrane suspended on top of a c-silicon substrate with Si pillars in between to stabilize the structure. The chip $(1.5 \times 1.5 \text{ cm}^2)$ comprises of several

trenches of the same trench height ($H \approx 500 \, \text{nm}$) but varying depths ($L \approx 5000, \, 1000, \, 520, \, 120, \, 70, \, \text{and} \, 40 \, \mu \text{m}$) and thus varying aspect ratios ($AR \approx 10 \, 000, \, 2000, \, 1040, \, 240, \, 140, \, \text{and} \, 80$). A side view of an LHAR trench is shown in Fig. 1. Once deposited, the polysilicon membrane can be peeled off revealing the deposition on the underlying c-Si substrate. A reference silicon substrate was also placed in each of the depositions alongside the LHAR trenches on which film thicknesses were measured right after depositions using spectroscopic ellipsometry. To do so, a three-layer stack with a bottom Si substrate, a middle native SiO₂ (2 nm), and a top alucone film modelled using Cauchy's dispersion relation was used.

MLD films are known to shrink within the first few hours upon exposure to the ambient due to reactions with moisture and oxygen. 14,15 Hence, in order to avoid any influence of ambient exposure on the measurements, we have intentionally exposed the film deposited within the LHAR trenches to the ambiance for more than 48h after which the alucone films are presumed to have reached a stable thickness. 14,15 The thickness profiles of the films were then measured using a Filmetrics F40 reflectometer. The setup is equipped with a "StageBase-XY10-Auto-100 mm" sample stage that can move in the x-y direction allowing to create thickness maps of the samples. The minimum step size in the stage movement allowed by the setup and the one used in this study is $4 \mu m$, and the spot diameter of the beam is $\sim 30 \,\mu\text{m}$. Film thicknesses were extracted by fitting the resulting reflected intensity versus wavelength data with the one derived using a model comprising of a bottom Si substrate and a top layer of the alucone film. The

Before deposition

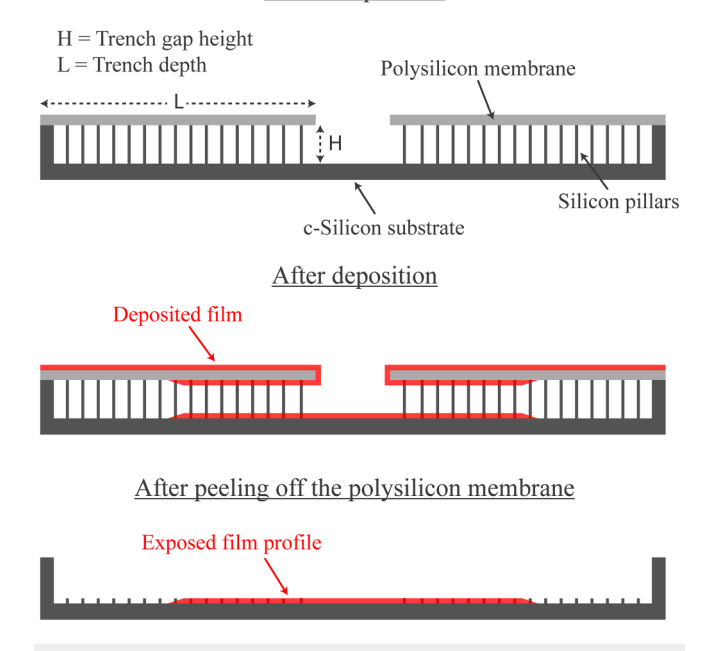


FIG. 1. Side-view schematic of the LHAR trenches used in this study. After deposition, the polysilicon roof over the trench is peeled off to reveal the film underneath. The revealed film profile is then mapped using reflectometry.

alucone film's refractive index was modelled using Cauchy's dispersion relation. In order to calculate the original thickness profiles of the films right after deposition, the film thicknesses measured on reference silicon substrates were used a reference to back-calculate the original profiles.

Anodized aluminum oxide (AAO) pores have also been used to inspect the conformality of alucone films on low-aspect-ratio structures. The AAO foils were supplied by InRedox and had an aspect ratio ranging from 3 to 5. Postdeposition, the AAO foils were bent by 180° revealing the pores at the crease, which were then imaged using a Hitachi SU70 analytical scanning electron microscope.

III. RESULTS AND DISCUSSION

A. Results

Figure 2 shows the thickness profile of an alucone film deposited inside a $1000\,\mu\mathrm{m}$ deep trench as measured by reflectometry. A TMA partial pressure of ~140 Pa and an EG partial pressure of ~67 Pa were used for deposition, and a dose time sequence TMA-purge-EG-purge of (0.77, 8.4, 0.77, and 2) was followed. The deposition was run for 225 MID cycles. The film thickness outside the trench (~77 nm) corresponds to a GPC of 0.34 nm/cycle, which is very similar to the GPC values previously observed on planar substrates under similar deposition conditions. Inside the trench, the film thickness initially increases to a maximum value of 120 nm at a distance of $56\,\mu\mathrm{m}$ from the trench entrance, followed by a decrease in thickness up to $180\,\mu\mathrm{m}$, where the film thickness reaches values below the reflectometry setup's resolution. Similar

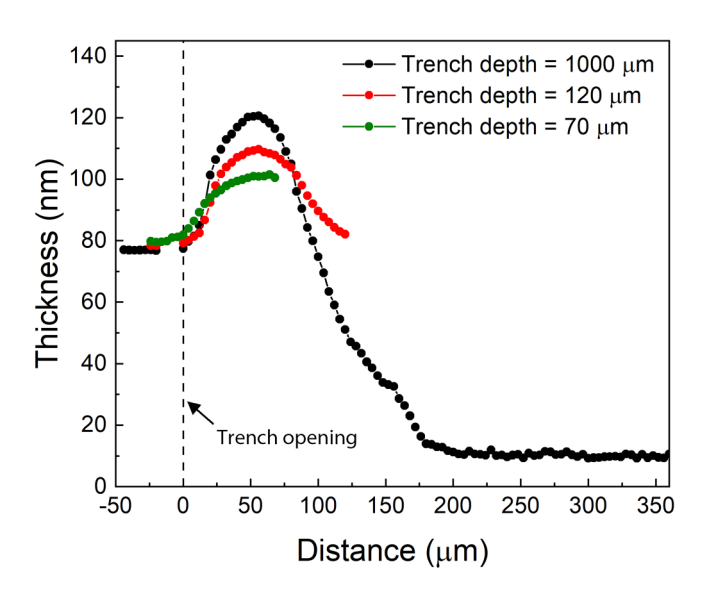


FIG. 2. Thickness profiles of the alucone films deposited using the same deposition conditions within LHAR trenches of different aspect ratios [same trench height (H) = 500 nm, varying trench depths (L) = 1000, 120, and $70 \,\mu\text{m}$] as measured by reflectometry. The thickness in each of the trenches is seen to increase until a distance $56 \,\mu\text{m}$ from the trench aperture after which it is found to decrease until the film penetration depth for 1000 and $120 \,\mu\text{m}$ deep trenches.

thickness profiles are observed for different trench depths, where the maximum thickness is observed to increase with the increasing trench depth. Additionally, the measured thickness profile inside the $1000\,\mu\mathrm{m}$ deep trench also appears to have a small shoulder around $150\,\mu\mathrm{m}$. The exact reason behind the shoulder is not known, but it was observed that the goodness of fit, which is an assessment of how well the simulated reflectivity fits the experimentally measured reflectivity of the sample, showed a decrease for the measurements around the shoulder. This suggests that the observed shoulder is likely a measurement artifact.

To investigate whether these thickness profiles are caused by TMA outgassing in combination with TMA and EG diffusion in the trench, a simple simulation model was constructed. Using MATLAB R2020a, we have simulated the purge step of TMA after its exposure step, during which the outgassing of TMA from the alucone films is accompanied by its simultaneous diffusion out of the LHAR trench. Trenches with varying depths and heights were modeled, each containing an alucone film with a uniform thickness penetrating until the end of the trench or up to a depth of $200\,\mu\text{m}$, corresponding to the experimentally observed maximum penetration depth seen in Fig. 2.

During the TMA exposure step, prior to the modeled purge step, TMA infiltrates into the alucone film, where the maximum TMA concentration in the film C depends on the TMA partial pressure $P_{\rm TMA}$ used during its exposure step and its solubility $S_{\rm t}^{17}$

$$C = S P_{\text{TMA}}. \tag{1}$$

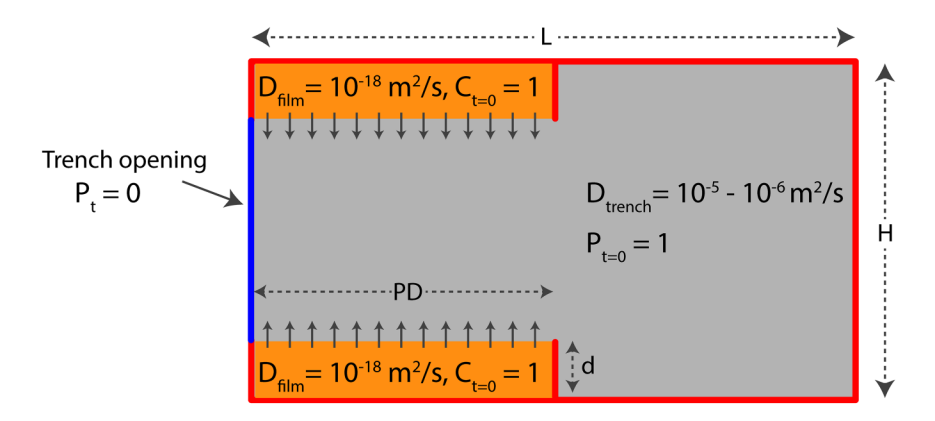
During the purge step, the outgassing rate "R" can be described as follows: 17

$$R = \frac{dC}{dt}\Big|_{\text{film surface}} = \alpha \cdot \left(P_t - \frac{C_s}{S}\right),\tag{2}$$

with C_s being the TMA concentration at the alucone film surface, α being a rate coefficient, and P_t being the TMA partial pressure in the trench after time t. Equation (2) is used as a boundary condition for the alucone film surface. For the uncoated trench walls, the boundary condition $\frac{dC}{dt} = 0$ is applied, and at the trench opening, the TMA partial pressure is fixed at zero ($P_t = 0$). Inside the trench and the alucone film, TMA is transported by diffusion using a diffusion coefficient value of 10^{-18} m²/s in the alucone film, while the diffusion coefficient in the trench can be approximated by the Knudsen diffusion coefficient, ranging from 10^{-5} to 10^{-6} m²/s depending on trench height (H) and deposited film thickness (d). A set of simplified starting conditions has been used: $P_{t=0} = 1$ in the trench and $C_{t=0} = 1$ in the alucone film. The model geometry, boundary, and initial conditions are summarized in Fig. 3.

The values of S and α for TMA in alucone are unknown. Solubility and rate coefficients can be determined, e.g., using gravimetric methods like QCM. ¹⁸ In the current modeling, we are mainly interested in evaluating trends; therefore, we have set the value of both S and α as 1, as varying these values will not impact the trends and conclusions of the model.





L = Depth of the trench H = Gap height of the LHAR trench

Neumann boundary condition where
 TMA flux across the boundary (j,) = 0

PD = Penetration depth of the alucone film d = Thickness of the deposited alucone film

Dirichlet boundary condition where TMA partial pressure at the boundary (P_.) = 0

FIG. 3. Geometry of the model used for performing the simulations. The free volume of a LHAR trench and the alucone film are indicated. Also shown are the initial and boundary conditions that were used to perform the simulations where D_{film} = diffusion coefficient of TMA in the alucone film and D_{trench} = diffusion coefficient of TMA in the free volume of the trench.

Figure 4 shows the result of the simulation where we have extracted the TMA partial pressure profile at $\frac{1}{2}H$ as a function of distance from the trench aperture for a $1000\,\mu\mathrm{m}$ deep and $500\,\mathrm{nm}$ high trench after 5 s of TMA purge time. It is observed that from

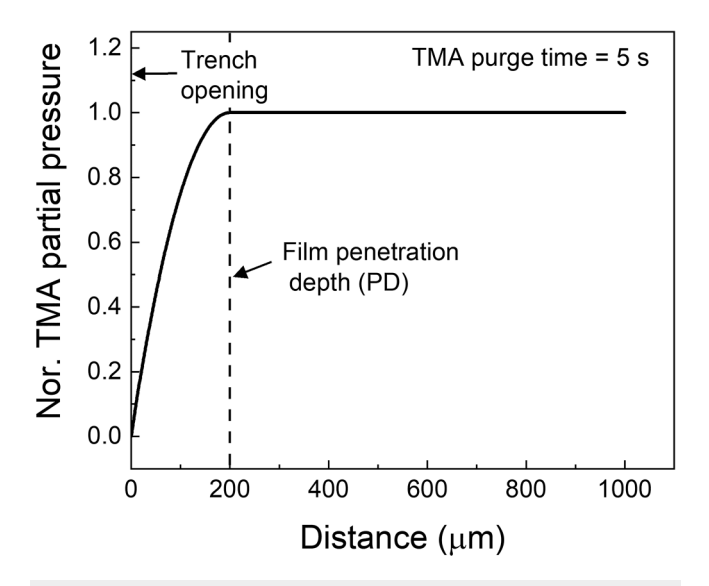


FIG. 4. Partial pressure profile of TMA inside a 1000 μ m deep trench as extracted from the simulation after a purge time of 5 s where the partial pressure is found to increase until the film penetration depth after which it stays constant for the rest of the depth. The simulation was performed using initial concentrations, boundary conditions, and diffusion coefficients as described in Fig. 3.

the trench aperture up to the film penetration depth, the TMA partial pressure increases from close to zero to a constant value, and beyond the penetration depth, the TMA partial pressure remains constant. In case such a TMA vapor-filled trench would be exposed to an EG dose, gas-phase reactions between TMA and EG will lead to CVD growth. A simple calculation shows, however, that these gas-phase CVD reactions cannot explain the observed thickness profiles. Using an alucone film density of 1.75 g/cm³ and an aluminum weight percentage of 36% as evaluated in our previous work, 14 it can be calculated that approximately 2.3×10^{-5} moles of aluminum atoms are required per nm of alucone thickness deposited per m² area. For a deposition area corresponding to 200 µm penetration depth of the film that is deposited on the floor and roof of a $1000 \,\mu\text{m}$ wide trench, $9.3 \times 10^{-12} \,\text{moles}$ of aluminum atoms are required per nm of film growth. The TMA partial pressure in the trench during outgassing can never exceed the employed partial pressure during the TMA dose. Assuming a maximum of 140 Pa TMA partial pressure inside a $1000 \,\mu\text{m}$ deep, 500 nm high, and $1000 \,\mu\text{m}$ wide trench, $\sim 2 \times 10^{-17}$ total moles of TMA would be present inside the trench. This is equivalent to a film thickness of $\sim 2 \times 10^{-6}$ nm, which is much lower than the additional CVD component of the measured thickness. Therefore, the additional CVD component is likely to originate from the reactions between EG and outgassing TMA on or near the alucone film surface, where the alucone film serves as a reservoir for TMA.

After a given purge time, the TMA concentration profile at the film surface during the EG dose can be approximated by the TMA outgassing rate and is assumed to remain unchanged during the entire EG dose. It can be further assumed that the EG partial pressure variation in the trench follows the inverse trend of the TMA partial pressure variation seen in Fig. 4, i.e., decreasing from



a fixed EG partial pressure at the trench opening to a zero partial pressure near the maximum penetration depth. The profile can be approximated using a complementary error function, which is a solution to Fick's diffusion equation for a semi-infinite medium.¹⁷

Next, the reaction rate R of the near-surface CVD reactions between EG and TMA and the deposited film thickness R_{dep} will depend on the concentration, or partial pressure, of both EG and TMA,

$$R_{dep} = k [\text{TMA}]^a [\text{EG}]^b, \tag{3}$$

with k being the deposition rate coefficient, [TMA] and [EG] being the concentrations of TMA and EG, respectively, and a and b being the partial reaction orders, which are assumed to be unity here for the sake of simplicity.

Using Eq. (3), it is now possible to simulate the added thickness on top of the pure MLD GPC due to the surface CVD reactions inside the trench. Figure 5(a) shows the modeled TMA concentration at the film surface and an approximated profile of the EG concentration as a function of the distance from the trench aperture and the product of the two as a measure of the deposited film thickness. It can be clearly seen that a thickness profile similar to the experimental observation in Fig. 2 is obtained. When different trench depths are included in the model, it can also be seen that the maximum thickness decreases with the trench depth, especially when the trench depth is less than the maximum penetration depth of the film [Fig. 5(b)]. This is again in excellent agreement with the results in Fig. 2. For shallow trenches, i.e., when the entire trench depth is coated with the alucone film, the volume of the alucone film and with that the reservoir size of infiltrated TMA decreases with decreasing trench depth. Therefore, less TMA is available after the TMA purge step, leading to a smaller CVD component and less thickness in the thickness profile. It can also be observed in Fig. 5(b) that the position of maximum CVD component shifts toward the trench entrance with decreasing depth of the trench. This is, however, simply because the EG concentration profile used to calculate the CVD component is the same for all the trenches. In reality, the EG concentration profile will evolve with the surface concentration of TMA and will be higher for shallower trenches. It can, however, be concluded from the experimental results and modeling that in case of insufficient TMA purge time, continued outgassing of TMA from the alucone film at a rate determined by the local TMA partial pressure in the trench, will lead to surface CVD reactions that result in a thickness profile originating initially from the increasing TMA surface concentration until the maximum thickness after which the thickness decreases due to decreasing EG concentration.

Figure 6 shows the measured thickness profile of alucone films deposited inside a deep 1000 µm trench and a shallow 70 µm trench for 225 and 450 MlD cycles. As expected, the thickness outside the trench for the 450 cycle film is roughly twice that for the 225 cycle film (160 vs 80 nm), but the thickness profiles inside the trench look very different. For the 1000 µm deep trench and 450 MID cycles, it can be seen that the thickness increase is much sharper and reaches the maximum thickness at a much shallower distance when compared to the 225 cycles' film. In an LHAR trench, the alucone film is deposited on both the trench floor and the trench roof. This means that for a 160 nm thick film, the trench height is locally reduced from 500 to 180 nm. As the diffusion coefficient in these trenches has a considerable Knudsen regime component, 19 the effective diffusion coefficient will significantly reduce when the trench height reduces upon film deposition. This will have a direct impact on the diffusion of both EG and TMA in and out of the trench gap.

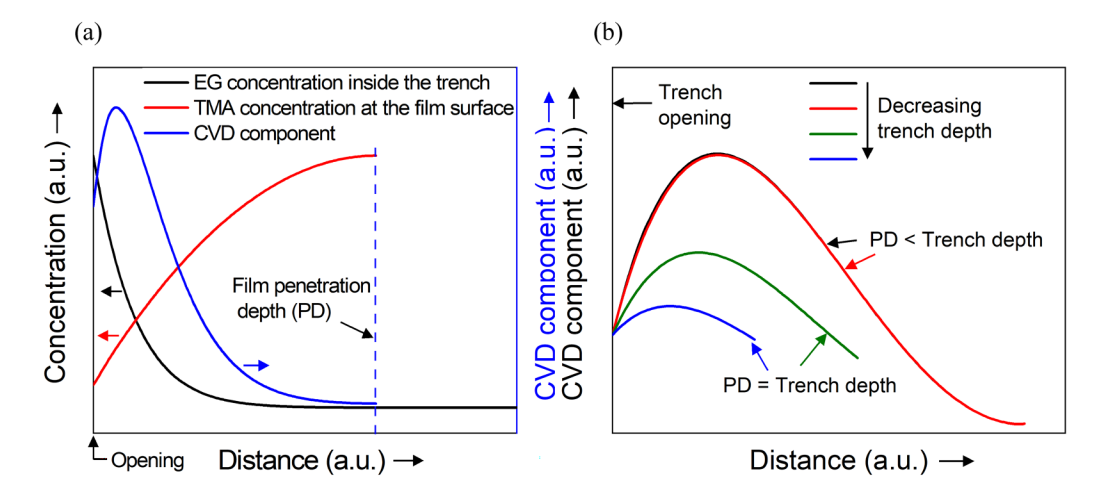


FIG. 5. (a) A schematic representation of the TMA concentration profile at the film surface and EG concentration profile inside the trench during the EG exposure step. The TMA surface concentration was taken to be proportional to its outgassing rate extracted at the film surface, while the EG concentration profile is approximated by a complementary error function, varying from a fixed concentration at the trench opening until zero at the film penetration depth. The resultant variation in the profile of the near-surface CVD component as calculated using Eq. (3) (k = 1) is also shown. (b) Schematic representations of the near-surface CVD component profiles for different trench depths.

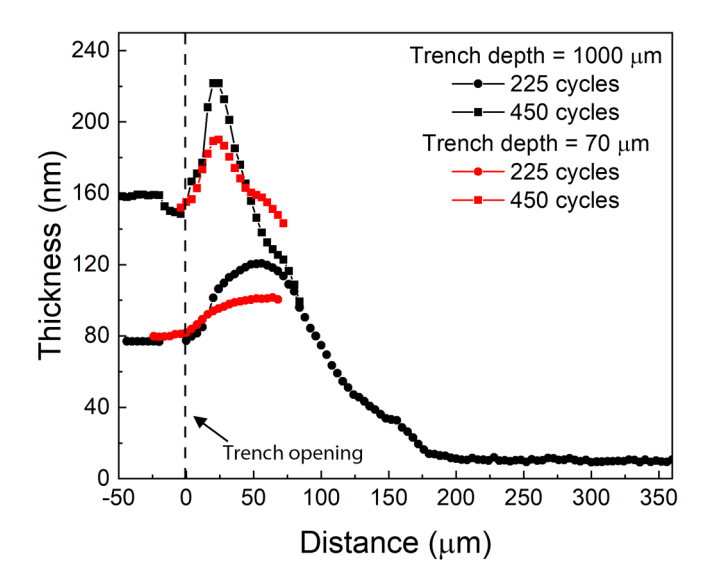


FIG. 6. Thickness profiles of alucone films deposited inside 1000 and $70\,\mu\mathrm{m}$ deep LHAR trenches using 225 MID cycles (filled circles) and 450 MID cycles (filled squares).

The effect of the trench height and, specifically, the diffusion coefficient was also simulated using the model described before. Figure 7(a) shows the simulated TMA partial pressure profile inside a 1000 µm deep trench with a 500 nm trench height corresponding to a diffusion coefficient of 10⁻⁵ m²/s, in comparison to a trench with a trench height of 50 nm corresponding to a diffusion coefficient of $10^{-6}\,\text{m}^2/\text{s}$. It can be seen in the case of the small trench height that the maximum TMA partial pressure is much higher than for the large trench height. A higher partial pressure of TMA means that the outgassing rate is reduced and more TMA is left inside the alucone film after the purge step. This is reflected in the modeled TMA surface concentration in Fig. 7(b). Figure 7(c) shows that the reduced Knudsen diffusion coefficient of EG leads to a larger EG partial pressure gradient near the trench opening as EG equally finds it difficult to diffuse into a narrow trench. The EG concentration profiles, similar to Fig. 5(a), are again approximated using complementary error functions using similar diffusion coefficients as for TMA. The larger gradients in TMA surface concentration and EG concentration inside the trench result in a higher value of the maximum CVD component for the trench with 50 nm trench height as compared to the trench with 500 nm trench height, while the position of the maximum CVD component shifts toward the trench opening [Fig. 7(d)] as the trench height gets smaller, explaining the experimental observations in Fig. 6.

Figure 6 also shows that for a 70 µm trench and 225 MlD cycles, a super-conformal thickness profile is obtained meaning that the coverage exceeds 100%. This can be explained by the fact that the trench depth is smaller than the maximum penetration depth obtainable by the EG and TMA doses and that the EG dose is sufficient enough to satisfy its surface reactions with TMA until the end of the trench. However, when the number of MLD cycles is

increased and thereby the trench height is decreased, a maximum in the thickness profile again appears before the end of the trench, following the same trend as for the $1000\,\mu\mathrm{m}$ deep trench. This is likely due to the above-explained effect of reduced trench height on the diffusion coefficients of TMA and EG.

To summarize, the surface CVD reactions that occur at the alucone surface in a trench lead to nonconformal thickness profiles that initially increase reaching a maximum and then decrease with increasing distance from the trench entrance. The maximum film thickness and the position where it is achieved depend on TMA and EG doses, TMA purge time, and the trench depth, but the maximum thickness position also shifts toward the trench opening as the trench height reduces upon continuous deposition. If the deposition is continued even further, the films deposited on both the trench walls (top and bottom) will meet and seal off the trench somewhere before the trench opening, resulting in a void. A simple simulation can be used to explain and describe these effects qualitatively, but more detailed modeling is required to quantitatively predict the dynamic behavior of the thickness profile during progressive MLD cycles.

B. Discussion

In cases where highly conformal MLD films in high aspect ratio structures are required, the thickness profiles observed in this work are clearly undesirable. The classical approach to suppress the undesirable effects of TMA outgassing and CVD reactions is to use extremely long TMA purge times. To fully outgas from planar alucone films, TMA purge times of up to 100 s of seconds are required.⁶⁻⁹ For 3D substrates, the required purge times will likely be even longer and probably increase with an increasing aspect ratio. These extremely long purge times might lead to uneconomical processes because of the resulting low deposition rates. It might, however, be possible to use shorter purge times as well as make use of the additional CVD GPC to increase the deposition rate. An adaptive cycling scheme that is based on varying the TMA and EG dose times and the TMA purge time with the increasing number of cycles to keep the thickness profile development under control can be adopted. To do this, a detailed understanding of the CVD component dynamics and its dependence on process conditions is required, preferably combined with in situ measurement of thickness profile evolution during cycling. This would be practically quite challenging. Furthermore, only one deposition temperature (150 °C) was explored in this entire study. This was decided based on our previous study on planar Si substrates where an in-depth effect of TMA and EG partial pressure on the CVD component was studied at the same temperature.9 The effect of deposition temperature on the conformality of alucone films requires further investigation. As observed in Fig. 6, a superconformal coating can be realized inside shallow trenches, when the trench depth is smaller than the maximum penetration depth achievable for the used TMA and EG doses. This would lead to a roughly V-shaped thickness profile. Once the V-shaped profile is achieved, the TMA purge times can be gradually increased for each cycle to reduce the CVD component and avoid the shift in the position of the maximum thickness in the trench. One might also continue to deposit conformally on top of the previously deposited V-shaped

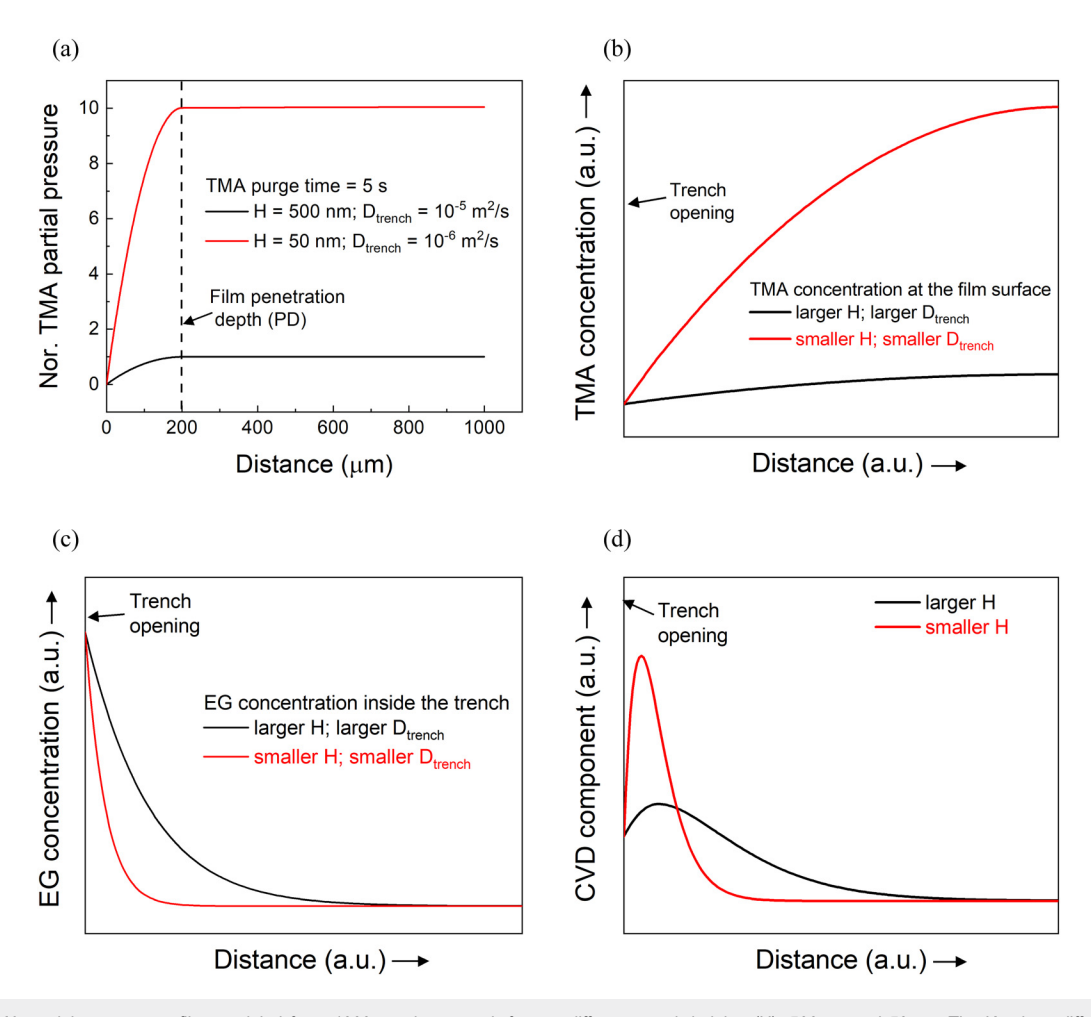


FIG. 7. (a) TMA partial pressure profiles modeled for a $1000 \, \mu m$ deep trench for two different trench heights (H): $500 \, nm$ and $50 \, nm$. The Knudsen diffusion coefficient varies with the trench height as indicated in the legend. The film penetration depth was fixed at $200 \, \mu m$. For two different trench heights, shown are (b) schematic representations of the TMA concentration profiles at the film surface after a given TMA purge time, (c) schematic representations of the EG partial pressure profiles inside the trench during the EG dose, and (d) schematic representations of the resultant CVD component profiles in the trench.

thickness profile by using very long TMA purge times, possibly leading to a void-free gap-fill, similar to when V-shaped trenches are used.²⁰

In our previous work, the use of DMAI instead of TMA has been proposed. 9,14 Although DMAI has a lower vapor pressure and reactivity than TMA, DMAI does not infiltrate into the underlying alucone film and long purge times are not required. As a result, significantly higher deposition rates on planar substrates were achieved using DMAI as compared to TMA. To investigate the conformality of alucone films prepared using DMAI, a deposition inside a $1000\,\mu\mathrm{m}$ deep LHAR trench was performed, and the thickness profile was measured (Fig. 8). The thickness of the DMAI + EG films outside the trench is close to 24 nm, which corresponds to a GPC of 0.053 nm/cycle, very similar to what was achieved on the accompanying silicon reference substrate. The GPC value is also very close to what has been previously reported. 14

Inside the trench, it can be clearly observed that the thickness of alucone films using DMAI is quite conformal up to a depth of ${\sim}200\,\mu\text{m}$. Also, the penetration depth of DMAI + EG films is much deeper than TMA + EG films. In TMA-prepared alucone depositions, the EG flux down the trench will deplete more rapidly due to CVD reactions. When using DMAI, the incoming EG will only be consumed by the pure MLD reactions and can, therefore, penetrate to deeper depths. In other words, DMAI might be a suitable alternative for TMA in MLD of alucone, not only on planar substrates but also when addressing high aspect ratio structures.

Finally, it is worth noting that the thickness profiles and the superconformal growth observed so far predominantly occur in high aspect ratio trenches. In very shallow trenches with an aspect ratio of <10, highly conformal alucone films can be deposited at high deposition rates by making use of the additional CVD component. Figure 9 shows SEM cross sections of low-aspect ratio

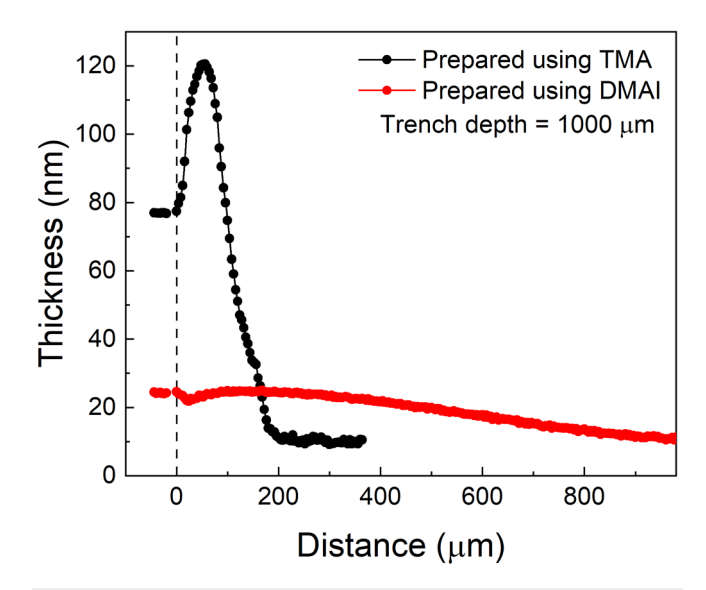


FIG. 8. Thickness profiles of alucone films deposited inside $1000\,\mu\text{m}$ deep LHAR trenches using TMA and DMAI as the aluminum precursors. The DMAI + EG deposition was carried out for 450 MLD cycles using a step-timing sequence of (0.77, 2, 0.77, and 8.4).

(between 3 and 5) AAO pores with alucone films deposited using TMA + EG and the same reactant partial pressures and step timings as the LHAR trenches for 50 (a) and 75 (b) MLD cycles. It can be observed that the growth of alucone films on low aspect ratio AAOs is quite conformal with the measured GPC (~0.32 nm/cycle) very close to what was observed on planar substrates (~0.34 nm/cycle). In the case of such low-aspect ratio structures, the outgassed TMA can quickly diffuse out of the pore and the concentration gradient of the gas-phase TMA along the pore depth is small. As a result, the outgassing rate of TMA and thereby the

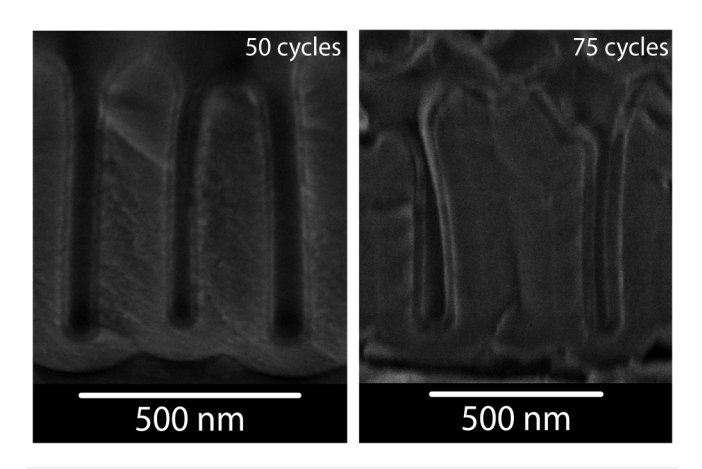


FIG. 9. Cross section SEM images of low aspect ratio AAOs coated with alucone films using a step timing sequence of (0.77, 8.4, 0.77, and 2).

CVD deposition rate are nearly constant along the entire pore depth, leading to conformal deposition, even with a CVD growth component.

IV. CONCLUSIONS

The infiltration of TMA into and its subsequent outgassing from alucone films occur not only on planar substrates but also when the alucone films are deposited inside 3D substrates. In this work, the conformality of alucone films deposited using TMA and EG inside high aspect ratio trenches was investigated at short TMA purge times. In such a scenario, the film growth inside 3D structures happens not just by the virtue of surface MLD reactions but also due to surface CVD reactions. The measured thickness profile of alucone films inside a 1000 µm deep and 500 nm high trench was found to be nonconformal with the thickness initially increasing with increasing distance from the trench entrance followed by a decrease until $180 \,\mu m$ after which no more film growth happens. The initial increase in thickness was mainly attributed to the increasing contributions from surface CVD reactions whereas the subsequent decrease was found likely to be due to decreasing EG concentration. The maximum thickness and the position where it is achieved in the thickness profile depend on both trench dimensions and deposition conditions, and simple simulations were used to explain the experimental observations in terms of reactant diffusion and reaction between EG and TMA inside the trench. Several options either to prevent or to benefit from surface CVD reactions have been discussed, where the use of DMAI as an alternative to TMA seems to be a suitable solution to deposit highly conformal alucone films inside high aspect ratio structures.

The results presented here clearly demonstrate the importance of looking beyond the precursor dose alone when investigating the conformality of an ALD or MLD process. The purge step can be of equal importance or sometimes of more importance in determining conformality, film properties, and deposition rate of ALD and MLD in high aspect ratio structures.

AUTHOR DECLARATIONS

Conflict of Interest

The authors have no conflicts to disclose.

Author Contributions

H.J. performed all the experiments mentioned in this work. The article was written with the help from P.P. and M.C.

Hardik Jain: Conceptualization (lead); Data curation (lead); Formal analysis (lead); Investigation (lead); Methodology (lead); Visualization (lead); Writing – original draft (lead). Mariadriana Creatore: Supervision (supporting); Writing – review & editing (supporting). Paul Poodt: Conceptualization (supporting); Data curation (supporting); Formal analysis (supporting); Funding acquisition (lead); Investigation (supporting); Methodology (supporting); Project administration (lead); Supervision (lead); Validation (lead); Writing – original draft (supporting); Writing – review & editing (lead).



ACKNOWLEDGMENTS

M.C. acknowledges the NWO Aspasia program. Erik Schuring and Xiaoqian Lu from TNO-Energy Transition are thanked for the sample preparation and SEM imaging of the AAO cross sections. This project has received funding from the European Union's Horizon 2020 research and innovation programme under the Marie Skłodowska-Curie Grant Agreement No 765378.

DATA AVAILABILITY

The data that support the findings of this study are available within the article and from the corresponding author upon reasonable request.

REFERENCES

- ¹V. Cremers, R. L. Puurunen, and J. Dendooven, Appl. Phys. Rev. 6, 021302
- ²P. Sundberg and M. Karppinen, Beilstein J. Nanotechnol. 5, 1104 (2014).
- ³M. Krishtab, I. Stassen, T. Stassin, A. J. Cruz, O. O. Okudur, S. Armini, C. Wilson, S. De Gendt, and R. Ameloot, Nat. Commun. 10, 1 (2019).
- ⁴X. Meng, J. Mater. Res. 36, 2 (2021).
- ⁵J. Multia and M. Karppinen, Adv. Mater. Interfaces 9, 2200210 (2022).

- ⁶A. A. Dameron, D. Seghete, B. B. Burton, S. D. Davidson, A. S. Cavanagh, J. A. Bertrand, and S. M. George, Chem. Mater. 20, 3315 (2008).
 Y. Lee, B. Yoon, A. S. Cavanagh, and S. M. George, Langmuir 27, 15155 (2011).
- ⁸D. Seghete, R. A. Hall, B. Yoon, and S. M. George, Langmuir 26, 19045 (2010). ⁹H. Jain and P. Poodt, <u>Dalton Trans.</u> **50**, 5807 (2021).
- 10 D. L. Zara, F. Zhang, F. Sun, M. R. Bailey, M. J. Quayle, G. Petersson, Folestad, and J. R. van Ommen, Appl. Mater. Today 22, 100945 (2021).
 B. Gong, Q. Peng, and G. N. Parsons, J. Phys. Chem. B 115, 5930 (2011).
- ¹²S. Sayegh, J. H. Lee, D. H. Yang, M. Weber, I. Iatsunskyi, E. Coy, A. Razzouk, S. S. Kim, and M. Bechelany, Sens. Actuators, B 344, 130302 (2021).
- 13P. Poodt, A. Lankhorst, F. Roozeboom, K. Spee, D. Maas, and A. Vermeer, Adv. Mater. 22, 3564 (2010).
- ¹⁴H. Jain, M. Creatore, and P. Poodt, Dalton Trans. **51**, 7918 (2022).
- 15K. Van De Kerckhove, M. K. S. Barr, L. Santinacci, P. M. Vereecken, J. Dendooven, and C. Detavernier, Dalton Trans. 47, 5860 (2018).
- 16 See https://www.filmetrics.com/thickness-measurement/f40 for information on the reflectometry setup's resolution (accessed 20 September 2022).
- ¹⁷J. Crank, *The Mathematics of Diffusion* (Clarendon, Oxford, 1975).
- ¹⁸A. Sinha, D. W. Hess, and C. L. Henderson, J. Vac. Sci. Technol. B 25, 1721 (2007).
- 19 P. Poodt, A. Mameli, J. Schulpen, W. M. M. (Erwin) Kessels, and F. Roozeboom, J. Vac. Sci. Technol. A 35, 021502 (2017).
- 20W. B. Wang, N. N. Chang, T. A. Codding, G. S. Girolami, and J. R. Abelson, J. Vac. Sci. Technol. A 32, 051512 (2014).